Hindawi Publishing Corporation
Advances in Materials Science and Engineering
Volume 2014, Article ID 274071, 12 pages
http://dx.doi.org/10.1155/2014/274071

Research Article

Acoustic Emission Measurement by Fiber Bragg Grating Glued to Cylindrical Sensor Holder

Masanori Takuma,[1] Shigeyoshi Hisada,[1] Kenichi Saitoh,[1] Yoshimasa Takahashi,[1] Yuuki Kobayashi,[2] Akira Kadono,[2] Atushi Murata,[2] Satoshi Iwata,[2] and Toshinori Sasaki[2]

[1] *Department of Mechanical Engineering, Kansai University, Yamatecho 3-3-35, Suita, Osaka 564-8680, Japan*
[2] *Graduate School of Engineering, Kansai University, Yamatecho 3-3-35, Suita, Osaka 564-8680, Japan*

Correspondence should be addressed to Masanori Takuma; t940081@kansai-u.ac.jp

Received 10 October 2013; Revised 11 December 2013; Accepted 12 December 2013; Published 10 February 2014

Academic Editor: Noriah Bidin

Fiber Bragg grating (FBG) is an optical fiber sensor and is suitable for acoustic emission (AE) measurements of structures such as chemical plants that require water resistance, explosion proofing, and so forth, However, directionality has been a problem in conventional usage which glues the grating range of an FBG to the inspection surface. This study proposes a cylinder-FBG (C-FBG) sensor with the FBG glued to a cylindrical sensor holder. Effectiveness of the sensor was evaluated by characterizing directionality and frequency sensitivity of the sensor and by comparing the detected AE signals in a 3-point bending test of a carbon fiber reinforced plastic (CFRP) laminate against a conventional wide-band piezoelectric AE sensor. The features of the detected signals were similar to the signals detected by the wide-band AE sensor. These results show that it is possible to produce a wide-band cylindrical sensor without the directionality limitations of the conventional usage of FBG.

1. Introduction

The health of facilities such as chemical plants and power generating stations must be evaluated periodically [1–6]. However, it is preferable to continually monitor the conditions of structures which have grown old or are working under severe environmental conditions. Acoustic Emission (AE) is widely utilized for monitoring in such conditions [4–8]. However, measurement by piezoelectric AE sensors suffers from the influence of electromagnetic waves, the risk of ignition by short circuit, and so forth. This problem is avoided by using optical fiber sensors which are also explosion proof and immune to corrosion [4, 7–10]. Thus, various AE measurement methods using the optical fiber have been developed [3, 4, 7–20].

In particular, a group at Aoyama Gakuin University has developed a Mach-Zehnder measurement system with a phase-compensation feedback control circuit and reported that measurements with high sensitivity are possible [11]. They also proposed resonance type sensors where the sensing fiber is wound on a cylindrical holder. Applications of the above-mentioned system have been reported [12–14]. However, the shape and the dimensions of the holder are constrained because it is difficult to wind the fiber around holders with small diameters, restricting the manufacture of high-frequency or wide-band sensors.

This study uses fiber Bragg grating (FBG) that can simultaneously measure AE and strain by gluing the detector onto the inspection object [15–19]. However, directionality has been a problem in this method because FBG can only detect vibration along the fiber length and cannot detect vibration perpendicular to the grating length. This is improved by using a cylindrical design, resulting in cylinder-FBG (C-FBG) sensors, in which the sensing part (grating length) of the FBG is glued to a cylindrical holder. By using this method, the holder can vibrate with elastic waves from every direction. As a result, the C-FBG sensor can detect waves from all directions because the grating expands and contracts.

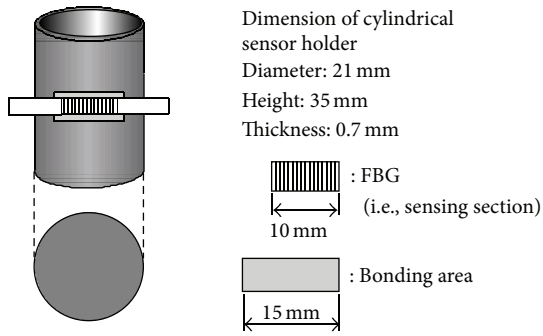

Figure 1: Dimension of C-FBG sensor. FBG is glued to a hollow cylinder with one closed end.

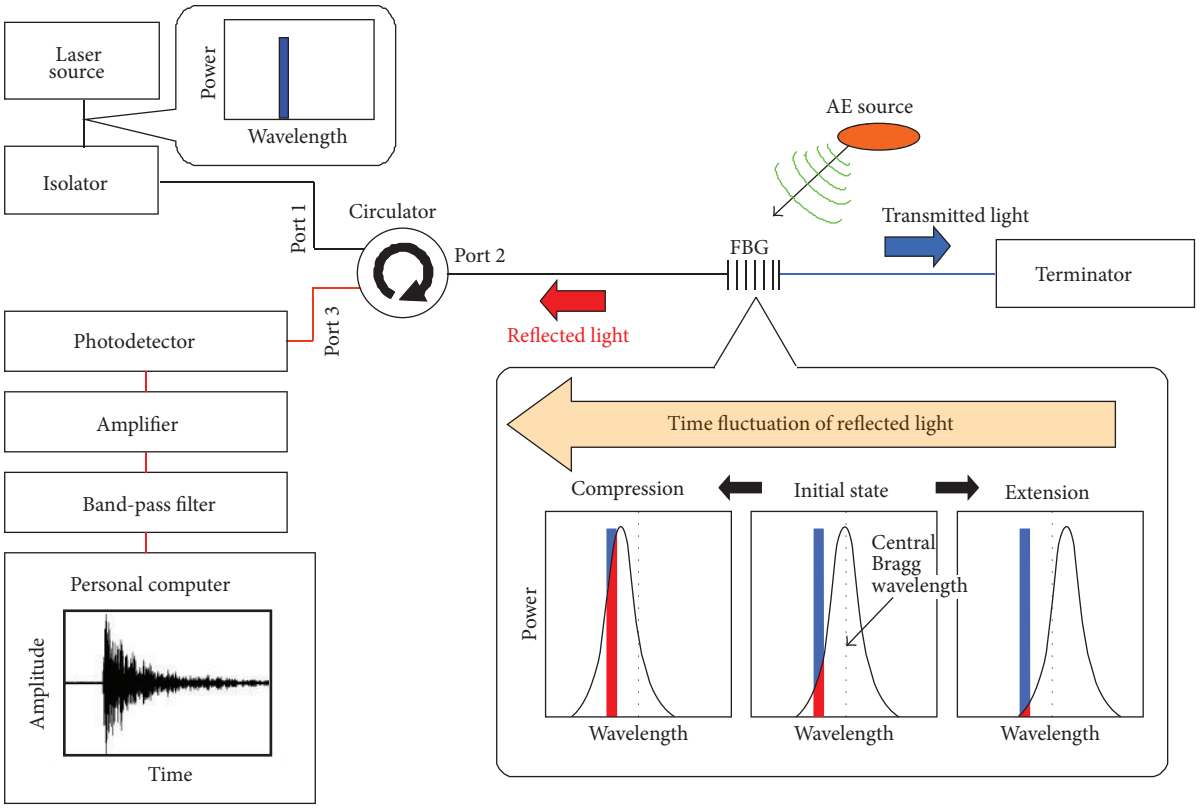

Figure 2: Measurement equipment for FBG. The central Bragg wavelength shifts right or left when the FBG is oscillated by the emitted elastic wave from the AE source. Then the energy in the region that overlaps with the central wavelength is converted into the electric signal. As a result, the elastic wave is detected.

2. Experimental Equipment and Methods

Several aspects of the proposed sensor first must be validated including directionality and frequency sensitivity. The proposed sensor is then compared to a conventional piezoelectric AE sensor using a 3-point bending test of carbon fiber reinforced plastic (CFRP) laminate.

2.1. C-FBG Sensor. Figure 1 shows the design of the proposed C-FBG sensor. Optical fiber (i.e., FBG) is glued to a hollow cylinder with one closed end. The closed end of the cylinder contacts the inspection surface by vacuum grease. The central Bragg wavelength of the FBG (Broptics Technology Corp.) is 1550 nm ± 0.2 nm with grating length of 10 mm. The entire grating length of the FBG is glued as shown in Figure 1 along with the dimensions of the cylindrical holder. The glued length is 15 mm. Because the end of the cylindrical holder minimizes the effect of large deformations of the inspection surface, the central Bragg wavelength does not undergo dramatic shifts. Consequently, the C-FBG can detect vibration with uniform sensitivity.

Figure 2 shows the measurement equipment for detecting the AE signals with FBG. The light from a laser source travels to an FBG via an isolator and a circulator. The shift

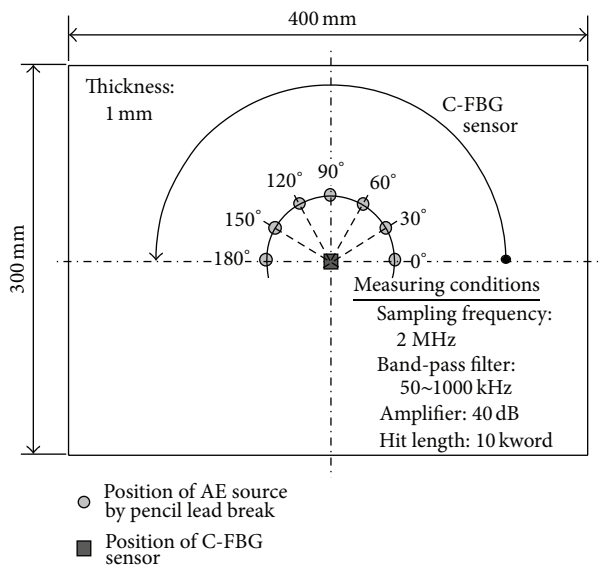

Figure 3: Evaluation for directionality of C-FBG sensor. The emitted elastic wave by pencil lead break at each position of circle mark is detected by a C-FBG sensor that was set at the position of the square. The directionality of the sensor is removed if the features of the detected waveforms at each position are similar.

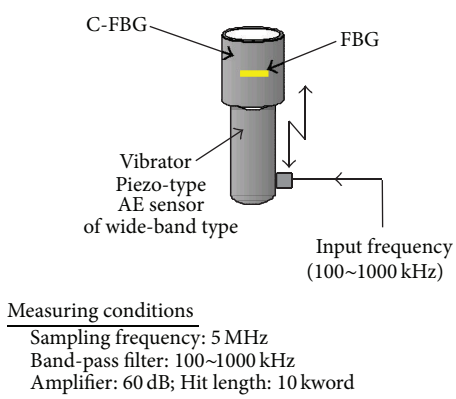

Figure 4: Evaluation for frequency sensitivity. Vacuum grease contacts both the vibrator and C-FBG sensor. It is concluded that the characteristic of C-FBG sensor is a wide-band type if the frequencies of the detected waveforms are similar to the input frequencies.

in central Bragg wavelength is positive or negative when the FBG is extended or compressed, respectively, by the ultrasonic vibration such as AE. The intensity of the reflected light changes according to the magnitude and direction of the wavelength shift. The transmitted and reflected light reaches a photodetector, and the Bragg shift is converted into a voltage signal [15–19]. The signal is stored in a personal computer via an amplifier and a band-pass filter.

2.2. Experiment on Directionality and Frequency Sensitivity Characteristics. The C-FBG sensor is glued to an aluminum plate. Using pencil lead breaks [21] at angle θ as shown in Figure 3, the ability of the sensor to detect these AE signals is evaluated. The diameter of lead is 0.5 mm. Directionality is evaluated by the S/N ratio where consistent S/N ratios at every angle θ indicate no influence of direction.

Figure 4 shows the scheme for evaluating the frequency sensitivity characteristics of the C-FBG sensor. The sensor and the vibrator contact each other as shown in the figure by vacuum grease. As the vibrator source, a wide-band piezoelectric AE sensor (AE-900S-WB: NF Corp.) with a relatively flat frequency characteristic was adopted, and the vibration face uniformly vibrates. Also, the frequency characteristics of the C-FBG sensor are evaluated by comparing the input and the detected frequencies. Here, the input frequencies to the vibrator range from 100 kHz to 1 MHz via a function generator, and the interval is 10 kHz. The C-FBG sensor detects the vibration of the transmitted sine wave from the vibration face. The frequency range was determined based

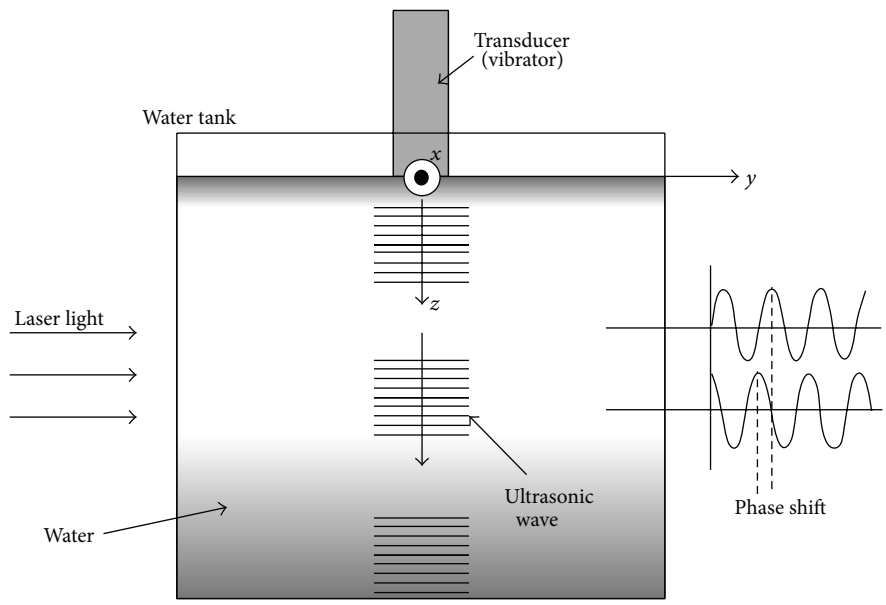

Figure 5: Basic configuration of holographic measurement of ultrasonic sound pressure.

on the guaranteed frequency characteristics of the adopted vibrator. The measuring conditions of the signals are shown in Figure 4.

In the evaluation of the C-FBG sensor sensitivity, the S/N ratio was used. The sensor is also evaluated by comparison of the input frequency and the detected frequency. Therefore, it is necessary to confirm whether the frequency f' of the function generator corresponds with the frequency f of the vibration face of the vibrator when the S/N ratio of the C-FBG sensor is evaluated with the method shown in Figure 4. Then, the frequency f was measured by the method shown in Figure 5. The technique uses optical acoustic imaging methods and is the visualization and the measurement method of the sound pressure distribution of ultrasonic waves by holographic interferometry where water is utilized as the pressure sensitive medium [22]. The simple explanation of this measurement theory is as follows.

The refraction index of water in the sound field changes by the sound pressure Δp of the ultrasonic wave when the wave oscillates in water. The optical path length of the laser beam (i.e., wavelength λ_L) changes by the refractive index variation when the laser beam is transmitted through the sound field. The optical path length change of the laser beam that is transmitted through the water is shown in the following equation where the z- and y-axes are the directions of the ultrasonic wave emission and the laser irradiation, respectively,

$$\int_0^L \left(\frac{dn}{dp}\right) \Delta p\,(x, y, z, t)\, dy = \frac{\lambda_L \Delta\phi\,(x, z, t)}{2\pi}, \qquad (1)$$

where $\Delta\phi(x, z, t)$ is the amount of phase shift at time t, L is the distance which the laser beam crosses across the sound field, and dn/dp is the refractive index variation of the water due to the pressure.

By the interference of the light wave transmitted through this field and the regeneration light wave of the hologram that recorded the condition without ultrasonic wave, a holographic interference fringe appears. The fringe is photographed by CCD camera. By fringe analysis, the distribution of the phase shift $\Delta\phi(x, z, t)$ is determined from the obtained interferogram as shown in Figure 6. It is possible to calculate the average sound pressure distribution $\Delta p(x, y, z, t)$ from the obtained $\Delta\phi(x, z, t)$ by (2) when the sound pressure distribution of the direction of the optical path L is uniform. Figure 6 is an example of the above-mentioned procedure. In the figure, the result of the frequency distribution with FFT results which processed the data is shown:

$$\Delta p\,(x, y, z, t) = \frac{\lambda_L \Delta\phi\,(x, z, t)}{2\pi L} \left(\frac{dp}{dn}\right). \qquad (2)$$

Figure 7 shows the relationship between the frequency of vibration face (i.e., the calculation results) and that of function generator (input). In this figure, the 45 degree line denotes when the input frequency of the function generator and the output frequency of vibrating surface of the vibrator agree perfectly. From this result, the frequencies of the generator correspond approximately to those of the vibration face as the correlation coefficient shows 0.9998. The maximum negative and positive errors are −7.837 and +19.959 kHz, respectively, at generator frequencies of 500 and 840 kHz, respectively. Therefore, the measured vibration face's frequencies were used as input frequencies f to the C-FBG sensors.

2.3. Three-Point Bending Test of CFRP Laminate. Figure 8 illustrates the experimental equipment for detecting AE

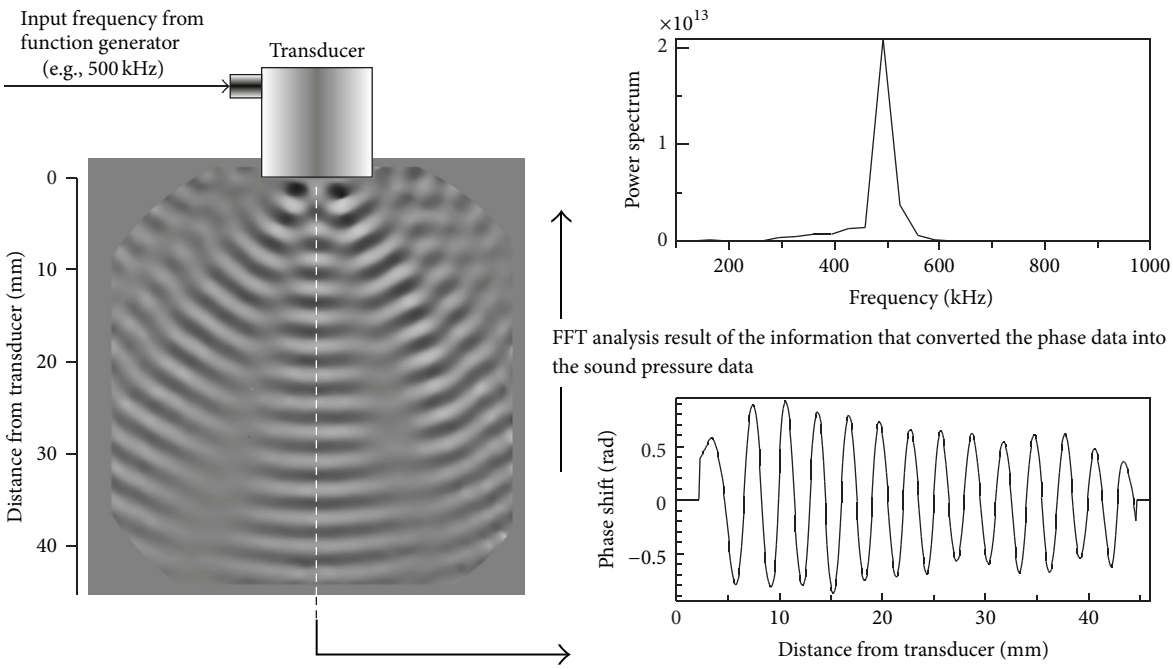

Figure 6: An example of fringe pattern analysis, phase shift, and its fast Fourier transform result.

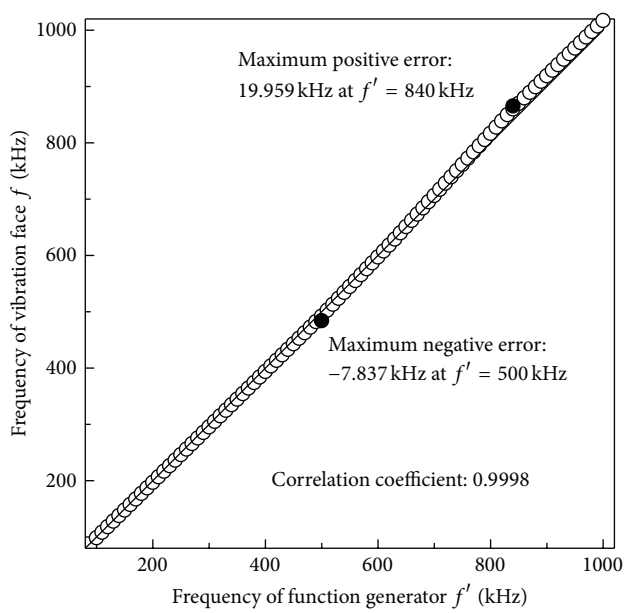

Figure 7: Comparison between frequencies of vibration face of vibrator and those of function generator. The data points fall on the 45 degree line when the input frequency of function generator and the output frequency of oscillating surface of the vibrator agree perfectly. The black circles denote the maximum negative and positive error.

signals during the bending test. Three sheets of plain woven fabric CFRP laminate (W-6101: TOHO TENAX Corp.) were used as the specimen. The rectangular dimensions of length, width, and thickness were 200 mm, 25 mm, and 0.85 mm, respectively.

The emitted AE signals during the test are detected by the C-FBG sensor and the wide-band piezo-electric AE sensor (AE-900S-WB: NF Corp.). The measurement conditions are shown in Figure 8. The amplifiers of both sensors are different because the sensitivity of piezo-type sensor is higher than the CFB sensor. Here, the indentation speed is 1 mm/min, and both sensors are glued by vacuum grease at the position of 50 mm from the indenter. The analysis results of each sensor are compared. Evaluation parameters and methods used are AE events, FFT, WMFD (weighted mean frequency distribution [23]), and WT (wavelet transform [24–26]).

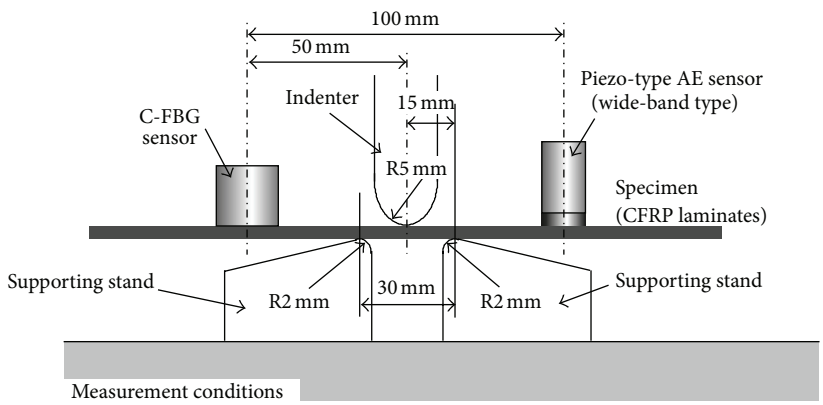

Measurement conditions

Kinds of sensor	Sampling frequency	Band-pass filter	Amplifier	Hit length
C-FBG	5 MHz	50~1000 kHz	50 dB	20 kword
Piezo-type (wide-band type)			30 dB	

Figure 8: Conceptual scheme of 3-point bending test. The amplifiers are different because the sensitivity of the PZT is higher than the C-FBG.

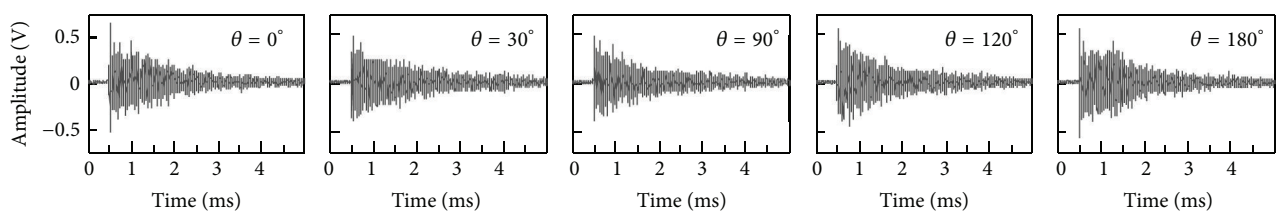

(a) Examples of detected AE waveforms by C-FBG sensor in Figure 3

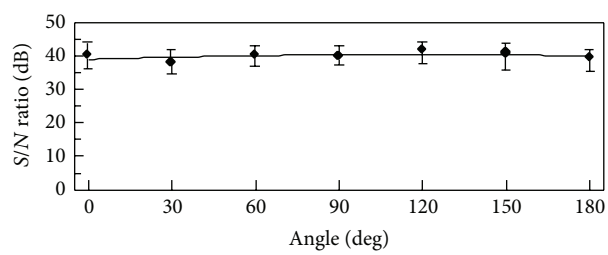

(b) S/N ratios of detected waveforms by C-FBG sensor in Figure 3

Figure 9: Evaluation of directionality of C-FBG sensor. The S/N ratios of the emitted waveform from each angle are shown. The directionality of the FBG was removed by using a cylindrical holder because the ratios are constant at each angle.

WMFD assembles many FFT analysis results into one result and is useful for extracting the features of the detection results. On the other hand, WT is a time-frequency analysis, enabling the capture of the generation time and the transition conditions of each frequency component.

3. Experimental Results and Discussion

3.1. Direction and Frequency Sensitivity Characteristics. Figure 9 shows an example of the S/N ratio of the detected signals at each incidence angle θ as defined in Figure 3. Here, twenty measurements were obtained at each angle. Figure 9(a) shows the detected waveforms, and the amplitude of the waveforms fluctuates minimally with changing angle. Therefore, it is estimated that the C-FBG sensor shows low directionality. Figure 9(b) shows the average of the S/N ratio of the detected waveforms. Therefore, it is also clear that the directionality of the FBG has been removed by the holder because the ratios are constant at every angle θ.

Figure 10(a) shows examples of the detected waveforms and their frequency analysis results with three input frequencies: 98.433, 492.163, and 918.900 kHz. Ten FFT analysis results were used for WMFD. The dots in WMFD results

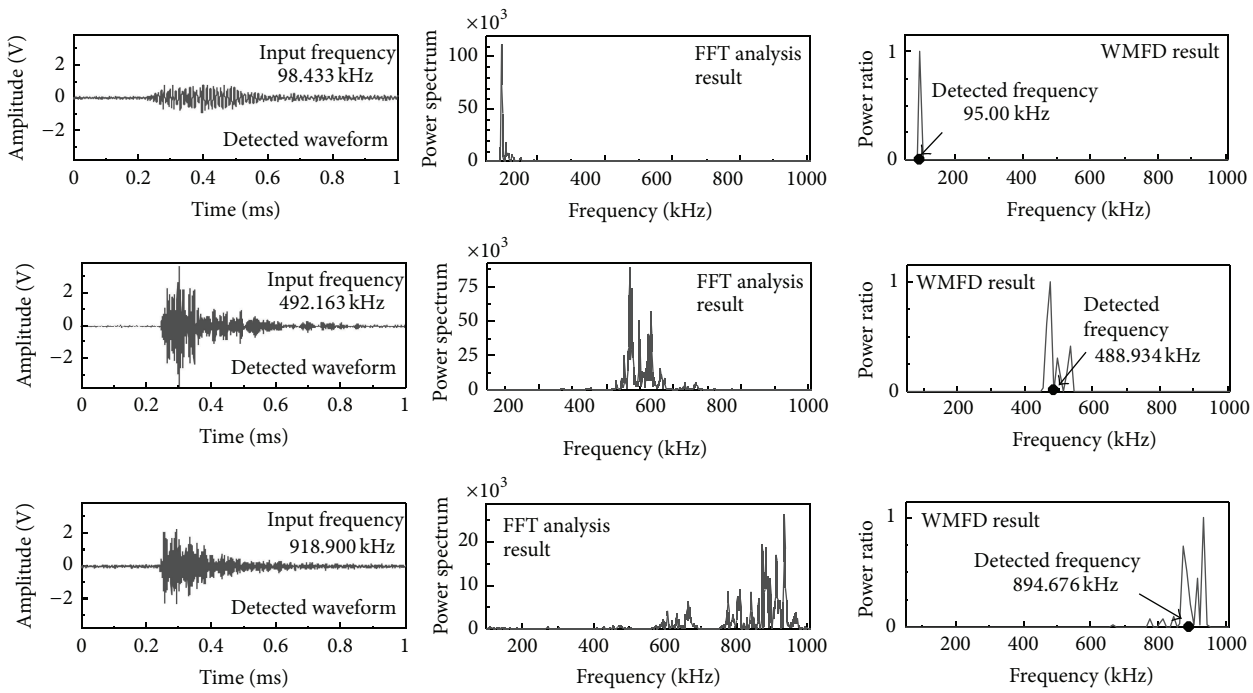

(a) Examples of detected AE waveform by C-FBG sensor at each input frequency, its FFT, and WMFD (large dot is the center of gravity position for frequency component in WMFD)

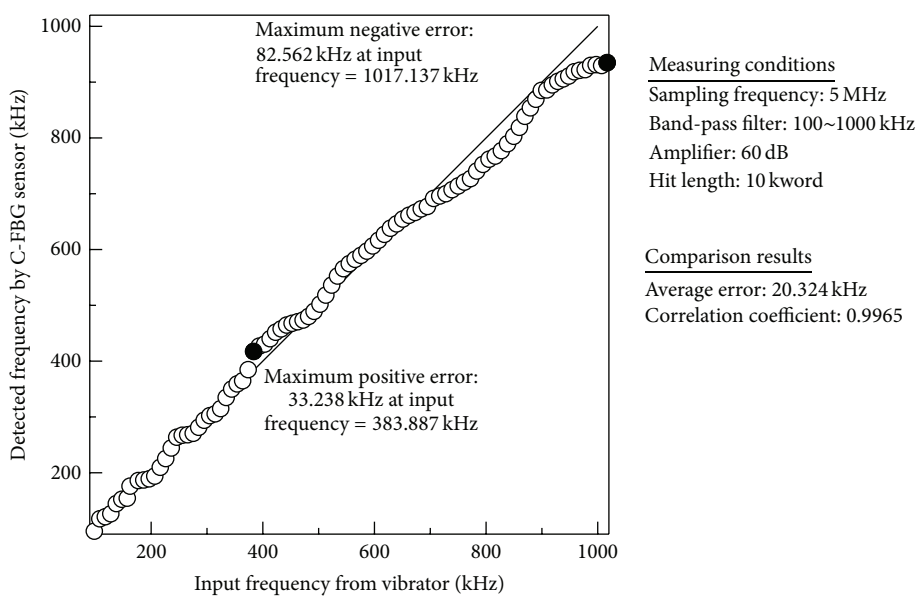

(b) Comparison of detected AE frequencies and input frequencies

Figure 10: Example of detected AE waveforms by C-FBG sensor and comparison of detected and input frequencies. The 45 degree line shown in (b) occurs when the C-FBG sensor accurately detects the input frequency. The black circles denote the maximum negative and positive error.

show the center of gravity on the frequency axis. The values show the relationship between input frequency and detected frequency; the detected frequencies are almost equal to the three input frequencies.

Figure 10(b) shows the relationship between the input frequencies to the C-FBG sensor from the vibrator and the frequencies detected by the C-FBG sensor. The plot indicates that the sensor detected the correct frequency as there are

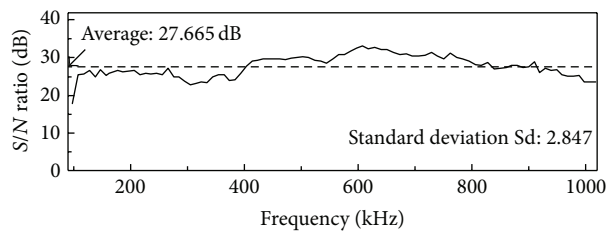

Figure 11: Frequency sensitivity characteristics of C-FBG sensor. The sensitivity for each frequency is evaluated by the S/N ratio. The character of the sensor is the wide-band type if the fluctuation is small. From the standard deviation and S/N ratio, the C-FBG sensor has the characteristics of the wide-band type.

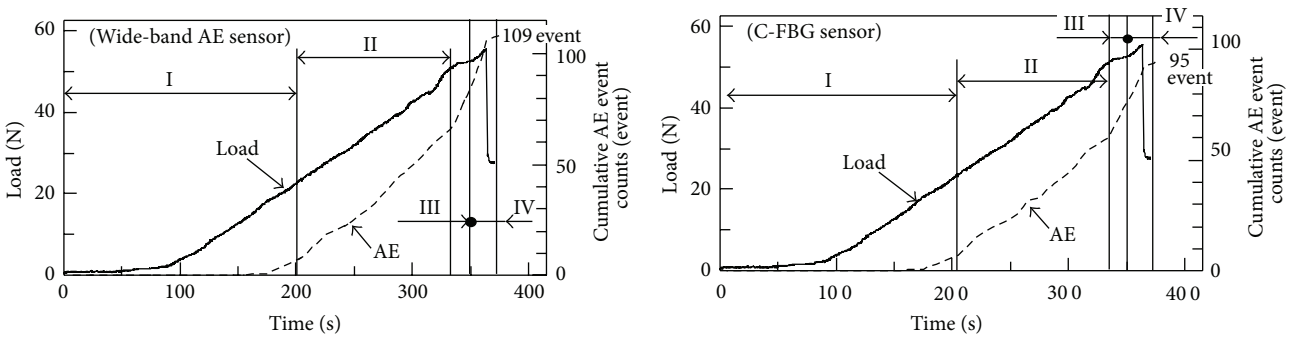

(a) Measurements of wide-band piezo-type AE sensor

(b) Measurements of C-FBG sensor

Figure 12: Relationship between load and AE event counts by each sensor in 3-point bending test of CFRP laminates. The continuous and broken lines show the load and the cumulative AE event count, respectively. The cumulative events detected by both sensors are similar. The cumulative event count of the PZT sensor (i.e., AE sensor) is higher than that of C-FBG sensor because the sensitivity of the former is higher than that of the latter.

many points along the 45° line at frequencies below 700 kHz (correlation coefficient is 0.9965). The maximum negative and positive errors are −82.562 and +33.238 kHz, respectively, at generator frequencies of 1017.137 and 383.887 kHz, respectively.

Figure 11 shows the frequency sensitivity of the C-FBG sensor using S/N ratios. From these results, the following things became clear. The S/N ratio does not fluctuate much from the mean, and the *Sd* is small (2.847).

From the results of Figures 10 and 11, the sensor shows features typical of wide-band sensors because the S/N ratios do not fluctuate at each input frequency, and the detected frequencies almost equal the input frequencies.

3.2. Results of Three-Point Bending Test of CFRP Laminate. In order to verify the accuracy of the AE measurements of the C-FBG sensor, the features of the detected signals by both sensors (C-FBG and the wide band piezo-type AE sensor) were compared.

Figure 12 shows the transitions of the cumulative AE event count and load in the testing, and they were classified into 4 regions. Here, the continuous and the dotted lines show the load and the count, respectively.

Region I: few AE events are detected.

Region II: the slope of the AE events line is greater than that in Region I, and the slope is similar to that of the load. This region continues, until the slope of the events line begins to increase further.

Region III: this region extends until 95% of the maximum load is achieved.

Region IV: the load begins to increase further and reaches the maximum value. This region continues, until the specimen fractures.

From the results, the events' counts by the C-FBG sensor are similar to those by the AE sensor.

Figures 13 and 14 show examples of the detected signal of each region shown in Figure 12 and its FFT, its WT result and WMFD in order to compare the frequency components of the signals for each sensor. The signals were detected at the same time by both sensors. The features of the components in the WMFD of the detected signals by the C-FBG sensor within each region are similar to those of the AE sensor. Therefore, these results show that the detected components in each region of Figure 13 resemble those in each region of Figure 14.

From the WT results of each region shown in Figures 13 and 14, it is considered that the character of both sensors is similar. The duration of the wavelets in the high frequency component (i.e., 200–700 kHz) is short, and that of the wavelets in the low frequency (i.e., 60–80 kHz) is long. The C-FBG sensor is able to grasp the time information of the emitted frequency components as well as the wide band

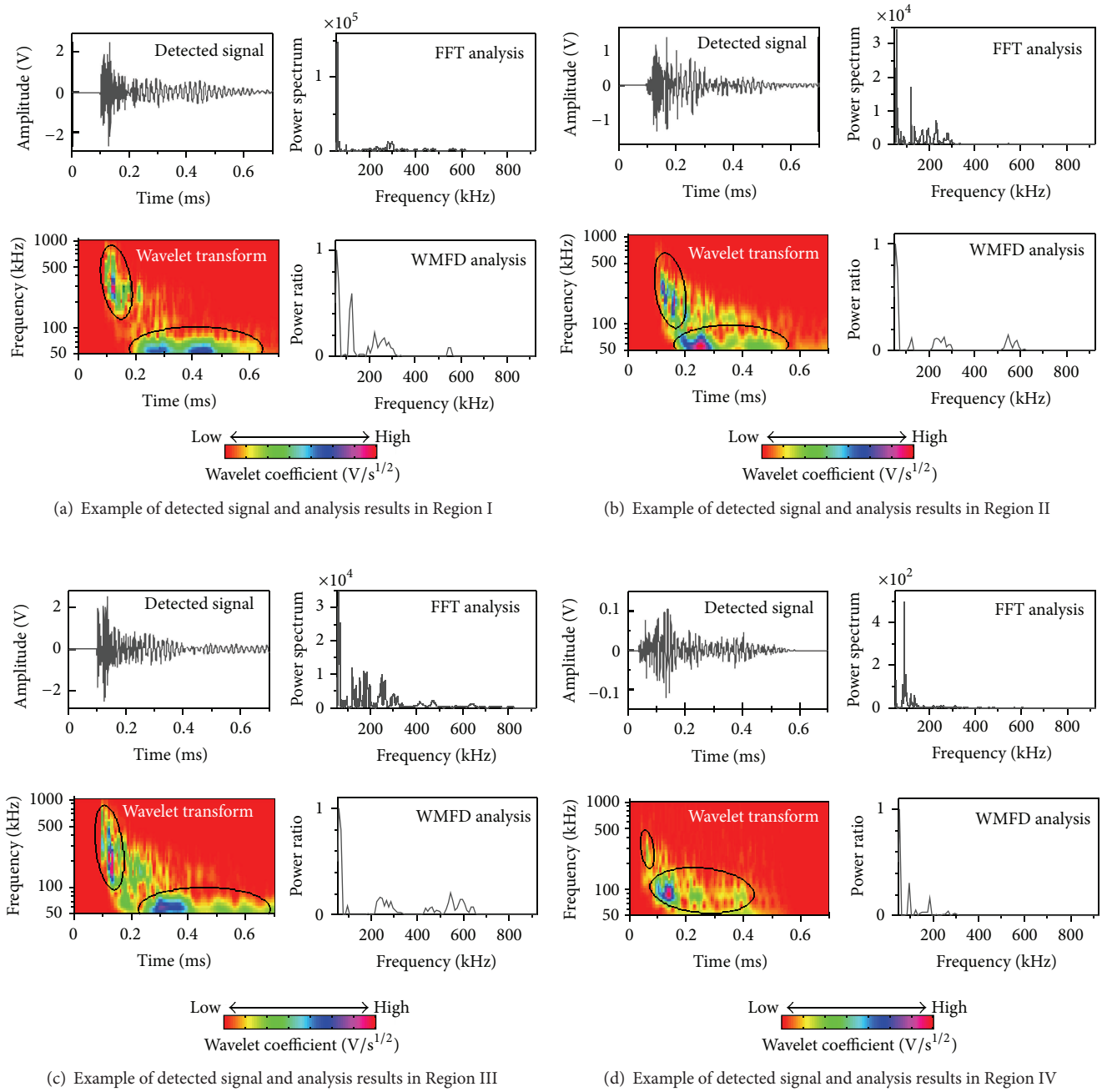

(a) Example of detected signal and analysis results in Region I

(b) Example of detected signal and analysis results in Region II

(c) Example of detected signal and analysis results in Region III

(d) Example of detected signal and analysis results in Region IV

Figure 13: Examples of detected AE signal by wide band piezo-type AE sensor and its FFT, its WT analysis, and WMFD in each region of the 3-point bending test in Figure 12(a).

piezo-type AE sensor. It is considered that the pattern by which the time fluctuation of the wavelet coefficient produces in each region of Figure 13 resembles that in each region of Figure 14.

In order to compare with the above results (i.e., Figures 13 and 14) and the analysis results of the detected signals by a piezo-type AE sensor of which the resonant frequency is 250 kHz (MICRO 30: PAC Corp.), the same bending test was carried out, and the AE signals were detected. Here, the measurement conditions were equal to the case in which the wide-band type sensor was adopted. Figure 15 shows the examples of the detected signal by the sensor within each region of the test and its FFT, its WT result and WMFD. From the observation results of the WT and WMFD, it is clear that only near 250 kHz which is the resonant frequency of the sensor is detected. These analysis results are clearly different from those results (i.e., Figures 13 and 14) by the sensors which showed the characteristics of wide-band type.

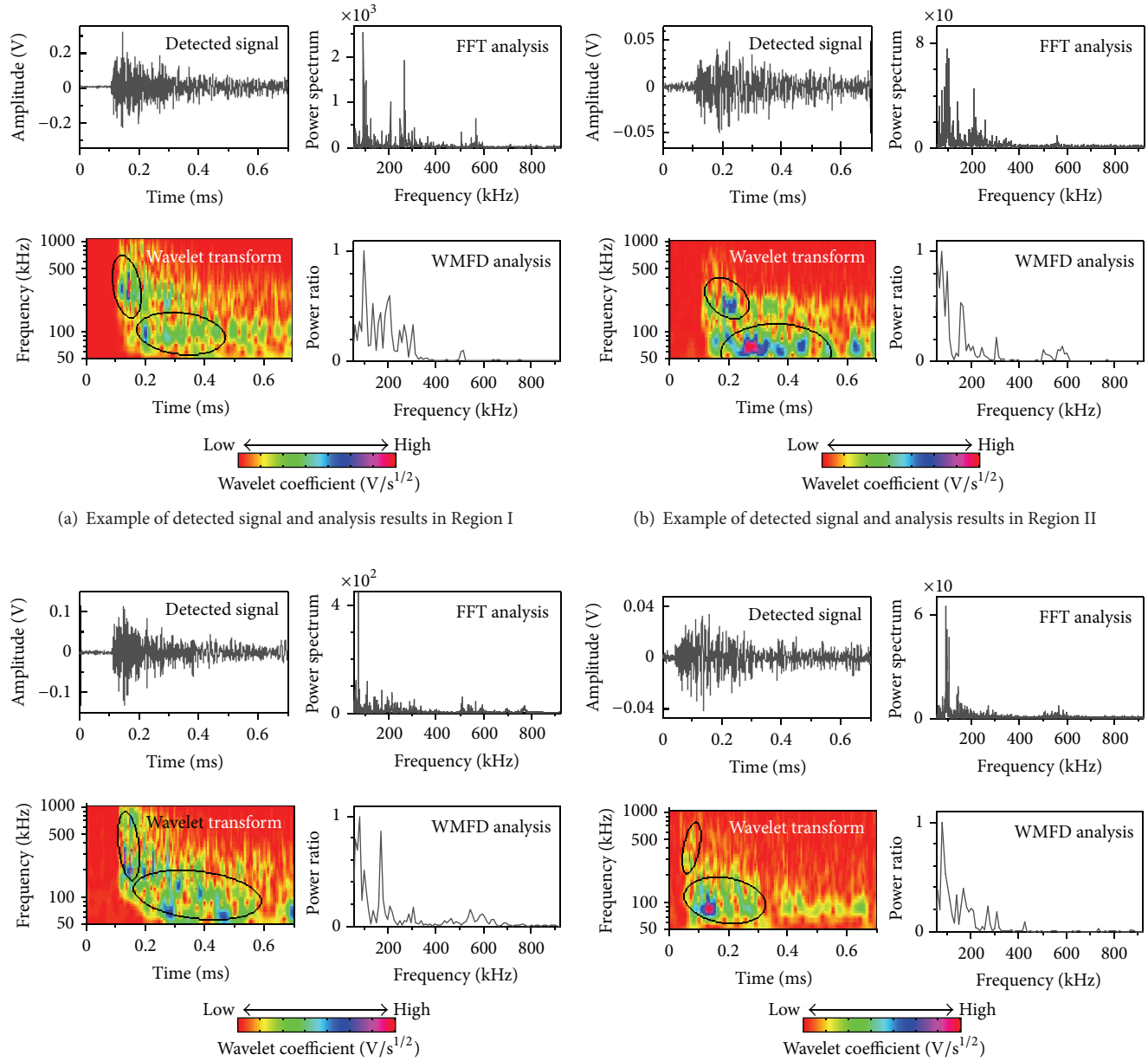

(a) Example of detected signal and analysis results in Region I

(b) Example of detected signal and analysis results in Region II

(c) Example of detected signal and analysis results in Region III

(d) Example of detected signal and analysis results in Region IV

Figure 14: Examples of detected AE signal by C-FBG sensor and its FFT, its WT analysis, and WMFD in each region of the 3-point bending test in Figure 12(b).

The above results show that it is possible to produce a wide-band C-FBG sensor by using FBG with good frequency sensitivity and nondirectionality and that is as effective as the AE sensor.

4. Conclusion

FBG is an attractive optical fiber sensor in AE measurements, but the conventional usage method that glues the sensor directly to the inspection surface has disadvantages such as directionality. In this study, the C-FBG sensor has an FBG glued to a cylindrical sensor holder, and the characteristics were evaluated through the experiments like the 3-point bending test of a CFRP laminate.

The C-FBG sensor is able to remove the directionality of an FBG glued directly to the detection surface. The characteristics of the S/N ratios of the input frequencies of the C-FBG sensor resemble those of a wide-band AE sensor. Also the frequency characteristics of the C-FBG sensor are equivalent to a wide-band piezo-type AE sensor. It is

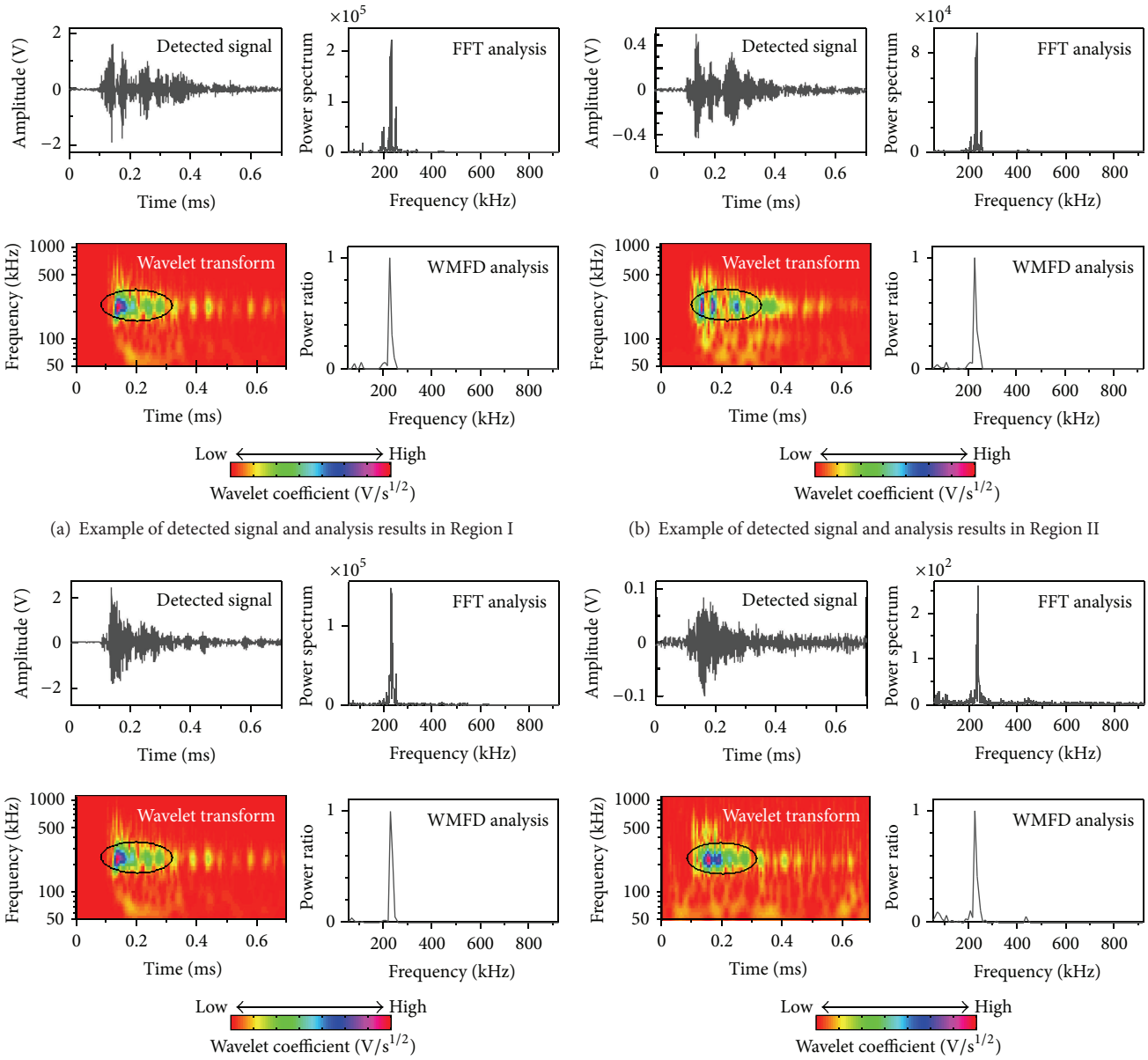

(a) Example of detected signal and analysis results in Region I

(b) Example of detected signal and analysis results in Region II

(c) Example of detected signal and analysis results in Region III

(d) Example of detected signal and analysis results in Region IV

Figure 15: Examples of detected AE signal by resonance piezo-type AE sensor (resonant frequency: 250 kHz) and its FFT, its WT analysis, and WMFD in each region of the 3-point bending test.

anticipated that the sensitivity of C-FBG sensor will approach that of the AE sensor if the amplification ratio or the laser power is increased. Also, it is possible that the various C-FBG sensor types will be produced by changing the shapes and the dimensions of the sensor holder. Hereafter, the produced C-FBG sensor will be subjected to material testing, and the ability of the sensors to evaluate damage to materials as well as AE sensor will be examined.

Conflict of Interests

The authors declare that there is no conflict of interests regarding the publication of this paper.

Acknowledgments

This research was financially supported by the Kansai University Grant-in-Aid for progress of research in graduate course, 2012.

References

[1] F. K. Chang, *Structural Health Monitoring 2003*, DEStech Publications, Lancaster, Pa, USA, 2003.

[2] H. Iwaki, H. Yamakawa, K. Shiba, and A. Mita, "Structural health monitoring system using FBG-based sensors for a

damage tolerant building," in *Proceedings of the 3rd International Workshop on Structural Health monitoring*, pp. 584–539, September 2001.

[3] S. Yashiro and N. Takeda, "A new approach for estimation of damage patterns in CFRP composite laminates using embedded FBG sensors," *Transactions of the Japan Society of Mechanical Engineers A*, vol. 71, no. 706, pp. 897–904, 2005.

[4] T. Matsuo, H. Cho, and M. Takemoto, "A new cascade multi sensor optical fiber AE system for the source dynamics and location," *Transactions of the Japan Society of Mechanical Engineers A*, vol. 72, no. 724, pp. 1895–1903, 2006.

[5] M. Takamoto, H. Cho, and H. Suzuki, "Lamb-wave acoustic emission for condition monitoring of tank bottom plates," *Journal of Acoustic Emission*, vol. 24, pp. 12–21, 2006.

[6] S. Yuyama, Z. Li, M. Yamada et al., "Noise analysis for acoustic emission evaluation of floor conditions in above-ground tank," *Journal of the Japanese Society for Non-Destructive Inspection*, vol. 53, no. 11, pp. 693–700, 2004.

[7] H. Yuki, H. Ishikawa, T. Iwamoto, and S. Ijima, "Development of acoustic emission sensor using transverse misalignment of optical fibers," *Journal of the Japanese Society for Non-Destructive Inspection*, vol. 53, no. 3, pp. 170–175, 2004.

[8] T. Matsuo, Y. Mizutani, H. Nishino, and M. Takemoto, "Source location of lamb AEs using optical fiber AE monitoring systems," *Journal of the Japanese Society for Non-Destructive Inspection*, vol. 52, no. 3, pp. 137–142, 2003.

[9] R. Tsuji, J. Mizusawa, Y. Maeda, and N. Aya, "Development of multipurpose sensor using Mach-Zehnder type optical fiber interferometer," IEICE Technical Report, Vol.104 507, 2004.

[10] H. Yuki, "Characteristics of Mach-Zehnder interferometer type optical fiber AE sensor," *Journal of the Japanese Society for Non-Destructive Inspection*, vol. 54, no. 2, pp. 66–69, 2005.

[11] H. Cho, R. Arai, and M. Takemoto, "Development of stabilized and high sensitive optical fiber acoustic emission system and its application," *Journal of Acoustic Emission*, vol. 23, pp. 72–80, 2005.

[12] T. Matsuo, H. Cho, and M. Takemoto, "Utilization of cascade optical fiber AE system for source location of lamb waves through a cross-ply CFRP plate," *Journal of Acoustic Emission*, vol. 24, pp. 84–96, 2006.

[13] T. Matsuo, H. Cho, and M. Takemoto, "Development of a new cascade multi-sensor optical fiber AE system," in *Proceedings of the Progress in Acoustic Emission XIII*, pp. 19–26, 2006.

[14] T. Matsuo, H. Cho, and M. Takemoto, "A new cascade multi sensor optical fiber AE system for the source dynamics and location," *Transactions of the Japan Society of Mechanical Engineers A*, vol. 72, no. 724, pp. 1895–1903, 2006.

[15] K. O. Hill and G. Meltz, "Fiber Bragg grating technology fundamentals and overview," *Journal of Lightwave Technology*, vol. 15, no. 8, pp. 1263–1276, 1997.

[16] H. Tsuda, "AE measurement using fiber Bragg gratings," *Journal of the Japanese Society for Non-Destructive Inspection*, vol. 52, no. 10, pp. 539–543, 2003.

[17] N. Takahashi, K. Yoshimura, S. Takahashi, and K. Imamura, "Development of an optical fiber hydrophone with fiber Bragg grating," *Ultrasonics*, vol. 38, no. 1–8, pp. 581–585, 2000.

[18] G. Wild and S. Hinckley, "Acousto-ultrasonic optical fiber sensors: overview and state-of-the-art," *IEEE Sensors Journal*, vol. 8, no. 7, pp. 1184–1193, 2008.

[19] H. Tsuda, "Development of fiber Bragg grating sensors for structural health monitoring," *Journal of the Japanese Society for Non-Destructive Inspection*, vol. 54, no. 2, pp. 71–75, 2005.

[20] H. Tamada, J. Kuwahara, Y. Okabe, N. Takeda, and S. Kojima, "Detection of delaminations in CFRP laminates by using FBG sensors as lamb wave receiver," *Transactions of the Japan Society for Aeronautical and Space Sciences*, vol. 53, no. 615, pp. 166–173, 2005.

[21] "The Japanese society for non-destructive inspection," Acoustic Emission, pp.22–23, (1990).

[22] S. Hisada, T. Suzuki, S. Nakahara, and T. Fujita, "Visualization and measurements of sound pressure distribution of ultrasonic wave by stroboscopic real-time holographic interferometry," *Japanese Journal of Applied Physics*, vol. 41, no. 5B, pp. 3316–3324, 2002.

[23] S. Somiya, T. Asano, and T. Sugiyama, "Relationship between frequency distribution characteristics of acoustic emission and fracture mechanisms on AFRP (2nd report, analysis of frequency distribution by weighted mean frequency distribution method)," *Transactions of the Japan Society of Mechanical Engineers A*, vol. 62, no. 598, pp. 1376–1381, 1996.

[24] H. Suzuki, T. Kinjo, Y. Hayashi, M. Takemoto, and K. Ono, "Wavelet transform of acoustic emission signals," *Journal of Acoustic Emission*, vol. 14, no. 2, pp. 69–84, 1996.

[25] E. P. Serrano and M. A. Fabio, "Application of the wavelet transform to acoustic emission signals processing," *IEEE Transactions on Signal Processing*, vol. 44, no. 5, pp. 1270–1275, 1996.

[26] H. Inoue, K. Kishimoto, T. Nakanishi, and T. Shibuya, "Time-frequency analysis of dispersive stress waves by means of wavelet transform (identification of group velocity and application to ultrasonic materials evaluation)," *Transactions of the Japan Society of Mechanical Engineers A*, vol. 61, no. 581, pp. 153–160, 1995.